Electronic Supplementary Information

Strategies for Regulating Pt-based H_2-SCR Catalytic Activity - Based on Alloying Effect

Wei Sun[a, †], Zhiqiang Wang[b, †], Qian Wang[a], Waqas Qamar Zaman[a], Limei Cao[a], Xue-Qing Gong[b,d], Ji Yang[a,c,d]

[a] *State Environmental Protection Key Laboratory of Environmental Risk Assessment and Control on Chemical Processes, School of Resources and Environmental Engineering. East China University of Science and Technology, 130 Meilong Road, Shanghai 200237, P.R. China.*

[b] *Key Laboratory for Advanced Materials, Center for Computational Chemistry and Research Institute of Industrial Catalysis, East China University of Science and Technology, 130 Meilong Road, Shanghai 200237, P.R. China.*

[c] *Shanghai Institute of Pollution Control and Ecological Security, Shanghai 200092, P.R. China.*

[d] **Corresponding author (*):** yangji@ecust.edu.cn; xgong@ecust.edu.cn.

Experiments and Methods

1. Materials preparation

The PtM alloy nanoparticle catalysts on carbon are prepared by the solvo-thermal method using the N,N-dimethylformamide (DMF) as the solvent and reductant. Firstly, 350 mg of carbon black (XC-72) mixed with 40 mL DMF solution and then ultrasonic dispersion to form homogeneous ink. For preparing PtM alloy nanoparticles, the precursors of different metals salt are $H_2PtCl_6 \cdot 6H_2O$, $Fe(NO_3)_2$, $Co(CH_3COO)_2$, $Ni(CH_3COO)_2$ and $Cu(CH_3COO)_2$, respectively. A certain amount of $H_2PtCl_6 \cdot 6H_2O$ and transition metals salts with 1:1 metal ions mole ratio are simultaneously added into the carbon black ink and ultrasonic dispersion for 30 min. Later the mixture is transferred into the Teflon pressure vessel. The reactors are loaded in an oven to heat at 170 °C for 12 h before it is cooled to room temperature. After that, the mixture is washed several times during filtration, followed under vacuum drying at 80 °C. Here, we will control the proportion of Pt in the total catalyst is about 8% (wt%).

2. Characterization of Catalyst.

The crystal structure of catalysts is investigated by means of powder X-ray diffraction (XRD) using a D/ max2550V apparatus with a Cu-Kα radiation source (λ = 1.5406 Å). The surface area of catalysts is determined by the Brunauer-Emmett-Teller (BET) method using Micromeritics Tristar 3020 SIN 993. The morphology of the catalysts is observed by mean of JEM-2100 transmission electron microscope (TEM). The compositions of catalysts are determined by Energy dispersive X-ray (EDX) spectrometer with a TEAMApollo system.

3. DFT Calculations

The first-principles calculations were performed using DFT methodologies implemented in the Vienna ab-initio simulation package (VASP)[1, 2]. The generalized gradient approximation (GGA) was used for the exchange–correlation functional in a form suggested by Perdew, Burke, and Ernzerhof (PBE)[3, 4], and a cutoff energy of 400 eV was used. Electron–ion interactions were treated with the projector augmented wave (PAW) method[5, 6]. Spin-polarized DFT calculations were applied in this study to obtain the lattice parameters, the total energies, and electronic structures for pure and doped Pt. The electronic charge analyses were conducted by Bader decomposition of the charge density.

Pt metals was chosen as the starting model to construct the binary metals of PtM (M = Pt, Fe, Co, Ni, Cu; mole ratio Pt:M = 1:1), and two Pt atoms in a cubic Pt bulk unit cell was substituted by two M atom (Fig. 1a). The calculated lattice parameters of PtM were obtained by optimizing the lattice constants with the fixed Pt lattice symmetry. The most common Pt (111) surface (Fig. 1b) was built as a slab model. Since our studies were mainly focused on the electronic effect of M on surface catalytic activity, the (111) surface with 2 × 2 supercell was modeled as periodic slab containing four layers. The bottom two atom-layers were kept fixed during calculations, while the other layers were allowed to relax. The force threshold of all the relaxed atoms was set to 0.05 eV/Å. The vacuum height of 12 Å between slabs was enough to eliminate the interaction between neighboring slabs. The Brillouin-zone integration was performed along with a 2 × 2 × 1 Monkhorst-Pack grid for the different surface slabs.

The adsorption energy (E_{ads}) was calculated as follows:

$E_{ads} = -(E_{total} - E_{substrate} - E_{gas\text{-}phase\ adsorbate})$

where E_{total} is the calculated total energy of the adsorption system, $E_{substrate}$ is the energy of the clean substrate and $E_{gas\text{-}phase\ adsorbate}$ is the energy of the gas-phase molecule. With these definitions, a positive value of Eads implies a release of energy or a stable adsorption on the surface.

We also consider the dispersion correction effect on the adsorption of H_2, and the dispersion correction that we main consider is Van der Waals force[7]. The related calculation method is as follows: the spin-polarized calculations were carried out with the DFT (PBE) - D3 (BJ) scheme as implemented in VASP. Default values of the dispersion coefficient (C6) and the vdW radii (R0) parameters given by Grimme were employed[8, 9].

4. H_2-SCR Reactor

According our previous studies, we use a fuel cell-like reactor to evaluate the H_2-SCR performance of prepared different PtM/C catalysts. The schematic of H_2-SCR reactor is shown in Figure S1. The reactor contains three parts, gas flow field on both sides and catalysts supported on carbon paper reaction layer in the middle. To prepare the reaction layer, 30 mg catalyst powder is added into 4 mL of isopropyl alcohol and 2 mL of deionized water, and ultrasonic to form homogeneous ink. After that, the mixture solution is spurt uniformly on both sides of carbon paper (size 5.5 cm × 5.5 cm). The concentration of NO and NO2 was continually measured using a chemiluminescent NO-NO2-NOx analyzer (Thermo Scientific, Model 42i). The conversion of NO was calculated using the following equation

$$DeNO = \frac{(C_{In} - C_{Out})}{C_{In}} \times 100\%$$

where C_{In} and C_{Out} depict the NO concentration in inlet and outlet of the reaction, respectively

Figures and Tables

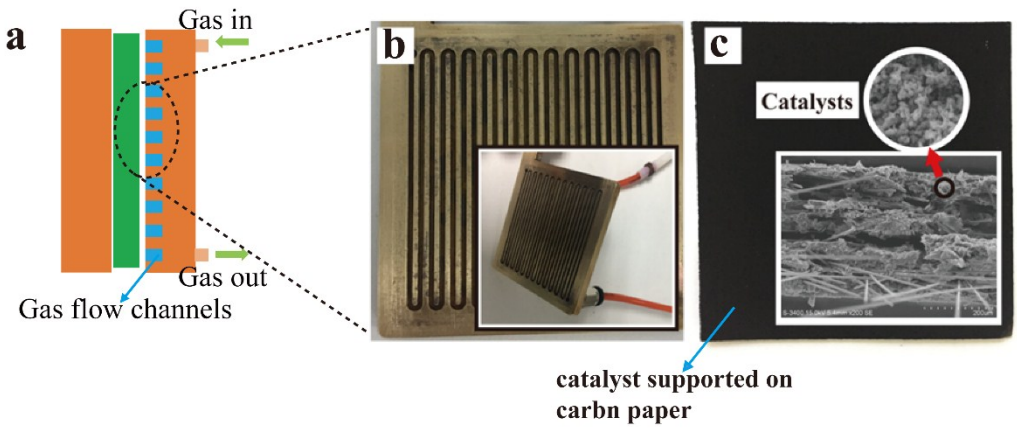

Figure S1. (a) The schematic of fuel cell reactor for H_2-SCR reaction. The midle is the reaction layer, where catalysts are supported on carbon paper. (b) The photo of reactor. (c) The photo of carbon paper supproted by catalyst. The insert is SEM section diagram image of carbon paper.

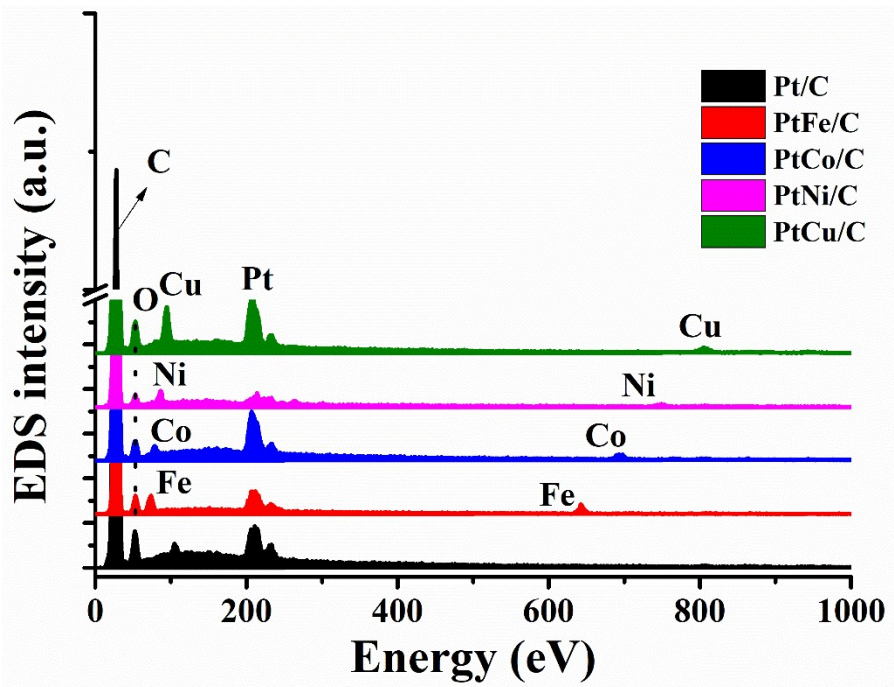

Fig S2. EDS spectra of prepared different PtM/C catalysts.

Table S1. The compositions of different PtM/C determined by EDS.

Elements	C (at%)	O (at%)	M (at%)	Pt (at%)	Pt/M
Pt/C	96.48	3.01	\	0.51	
PtFe/C	95.00	3.95	0.51	0.54	1.06
PtCo/C	95.86	3.19	0.46	0.49	1.07
PtNi/C	96.32	2.87	0.52	0.48	0.92
PtCu/C	95.79	3.13	0.56	0.52	0.93

Table S2. NO conversion comparison of different catalyst.

Catalysts	NO conversion (%)	Mass ratio of Pt (%)	Relative activity (based on Pt/C)
Pt/C	10 ± 3	8	1
PtFe/C	52.3 ± 4	6.22	6.17
PtCo/C	30.1 ± 5	6.14	3.56
PtNi/C	21.7 ± 4	6.14	11.83
PtCu/C	98.9 ± 1	6.03	2.64

Table S3. BET surface area of prepared different catalysts.

Materials	C	Pt/C	PtFe/C	PtCo/C	PtNi/C	PtCu/C
BET surface area (m^2 g^{-1})	229.3	201.4	199.2	213.1	201.1	188.6

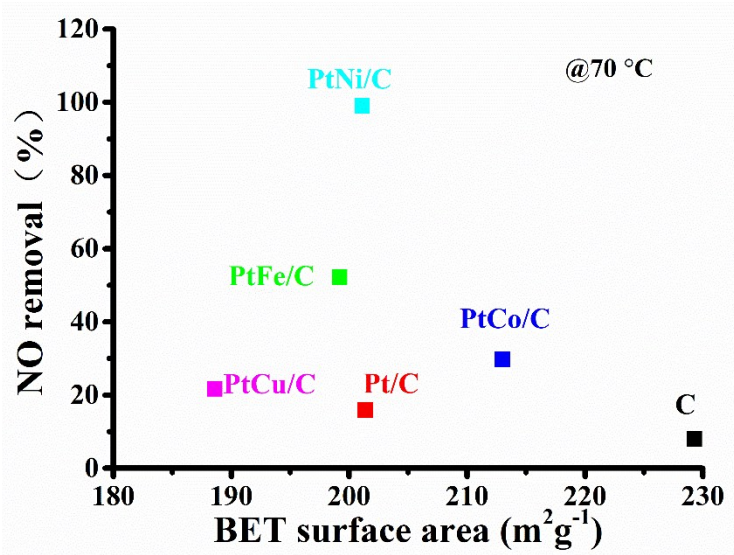

Fig S3. The relationship between BET surface area and NO removal.

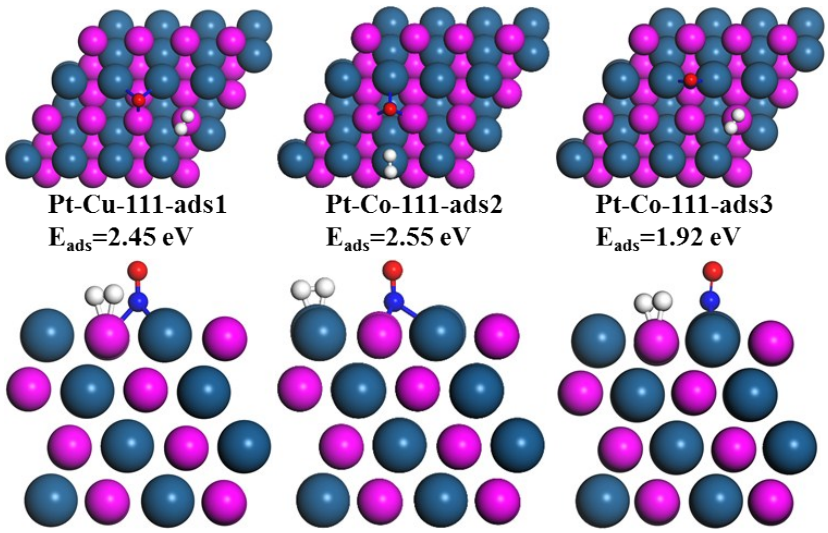

Fig S4. The structures and co-adsorption energies on different activity sites of PtCo(111) surface.

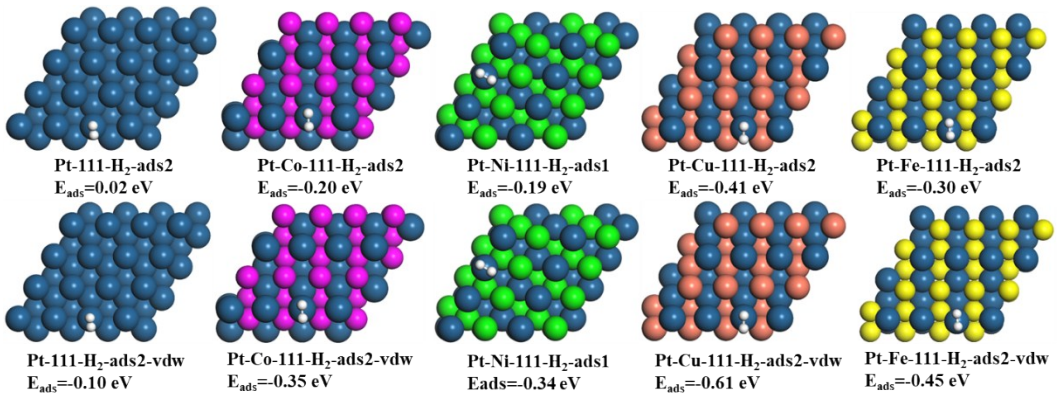

Fig S5. The structures and energies of hydrogen adsorbed on pure Pt and PtM (M=Co, Ni, Cu, Fe) alloy. Vdw means that the calculation adding the Van der Waals force.

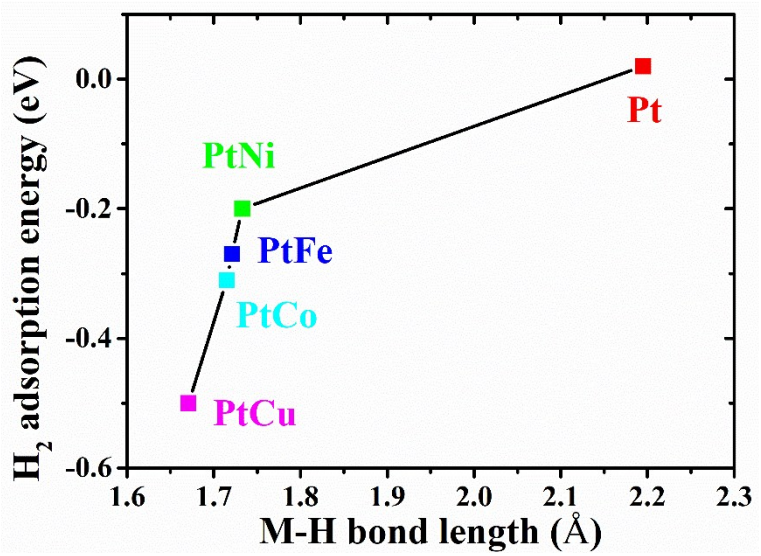

Fig S6. Relationships between M-H bond length and H_2 adsorption energy.

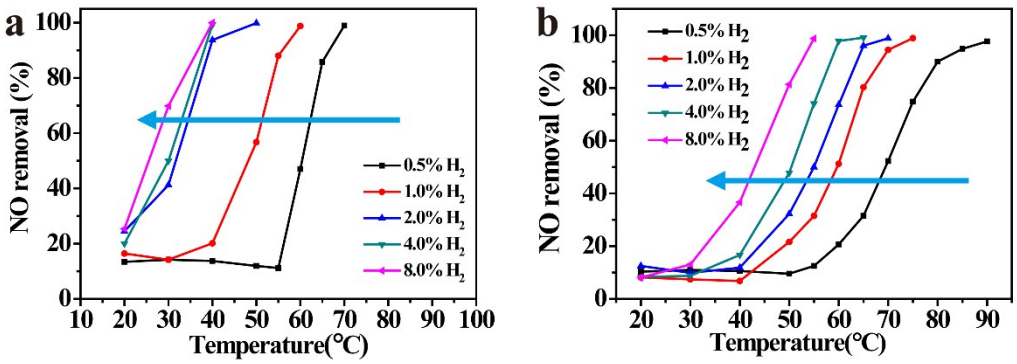

Fig S7. The effect of H_2 concentration on the catalytic activity of H_2-SCR. (a) is the PtNi/C and (b) is the PtFe/C. As shown in figure, with the increase of H_2 concentration in the gas flow, both of the initial temperature of reaction and the temperature of 100% removal will shift towards low temperature. It implies that the increase of H_2 concentration not only promoting the reaction kinetics, also enhancing the H2 adsorption.

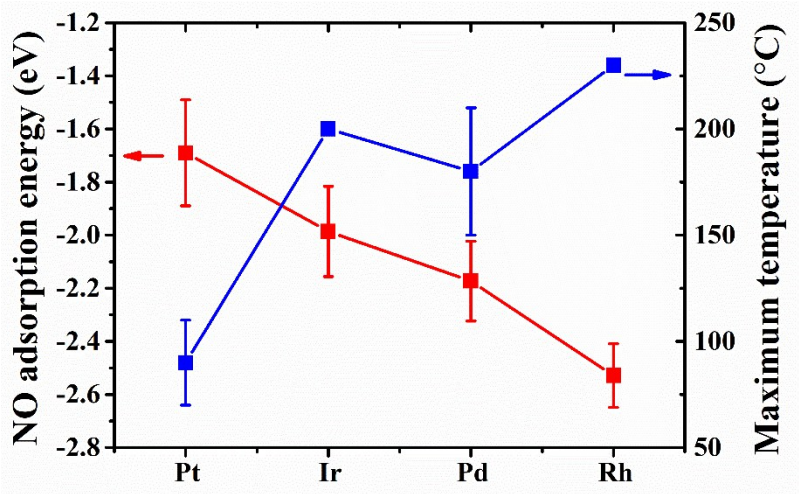

Figure S8. The calculated adsorption energies for NO on various metals[10-13], and the maximum reaction activity temperature of different metals[14]. It implies that the strong adsorption of NO will result in low catalytic activity.

Table S4. The lattice constant of different PtM alloy.

Sample	Pt	PtFe	PtCo	PtNi	PtCu	
DFT	3.93	a=3.842;c=3.791	a=3.888;c=3.507	a[15]=3.794;c=3.574	a=3.878	This work

EXP	3.92	a=3.826
		a[16]=3.866
		a[17]=3.859;
		a[18]=3.845
			a=3.858
			a[19]=3.82;
			a[16]=3.854;
			a[20]=3.844
				a=3.781
				a[16]=3.812;
				a[20]=3.817
				a[21]=3.741
				a[3]=3.849
					a=3.874
					a[22]=3.83;
					a[23]=3.873
					a[24]=3.89
					a[25]=3.80
					a[26]=3.76
						This work

Table S5. The M-N bond length of different Pt alloy.

Sample	Pt	PtFe	PtCo	PtNi	PtCu
Pt-N (Å)	2.077	2.254	2.131	2.127	2.187
M1-N (Å)	2.078	1.928	1.900	1.877	2.003
M2-N (Å)	2.078	1.932	1.894	1.875	1.985

References:

1. Kresse, G.; Furthmüller, J., Efficiency of ab-initio total energy calculations for metals and semiconductors using a plane-wave basis set. *Computational Materials Science* **1996,** *6*, (1), 15-50.
2. Kresse, G.; Furthmüller, J., Efficient iterative schemes for ab initio total-energy calculations using a plane-wave basis set. *Physical review B* **1996,** *54*, (16), 11169.
3. Perdew, J. P.; Wang, Y., Accurate and simple analytic representation of the electron-gas correlation energy. *Physical Review B* **1992,** *45*, (23), 13244-13249.
4. Perdew, J. P.; Burke, K.; Ernzerhof, M., Generalized Gradient Approximation Made Simple. *Physical Review Letters* **1996,** *77*, (18), 3865-3868.

5. Kresse, G.; Hafner, J., Ab initio molecular dynamics for open-shell transition metals. *Physical review. B, Condensed matter* **1993,** *48*, (17), 13115-13118.
6. Blöchl, P. E., Projector augmented-wave method. *Physical review B* **1994,** *50*, (24), 17953.
7. López-Corral, I.; Piriz, S.; Faccio, R.; Juan, A.; Avena, M., A van der Waals DFT study of PtH2 systems absorbed on pristine and defective graphene. *Applied Surface Science* **2016,** *382*, 80-87.
8. Grimme, S.; Antony, J.; Ehrlich, S.; Krieg, H., A consistent and accurate ab initio parametrization of density functional dispersion correction (DFT-D) for the 94 elements H-Pu. *The Journal of chemical physics* **2010,** *132*, (15), 154104.
9. Grimme, S.; Ehrlich, S.; Goerigk, L., Effect of the damping function in dispersion corrected density functional theory. *Journal of computational chemistry* **2011,** *32*, (7), 1456-1465.
10. Huang, X.; Mason, S., DFT-GGA errors in NO chemisorption energies on (111) transition metal surfaces: Possible origins and correction schemes. *Surface Science* **2013**.
11. Vang, R. T.; Wang, J.-G.; Knudsen, J.; Schnadt, J.; Lægsgaard, E.; Stensgaard, I.; Besenbacher, F., The adsorption structure of NO on Pd (111) at high pressures studied by STM and DFT. *The Journal of Physical Chemistry B* **2005,** *109*, (30), 14262-14265.
12. Popa, C.; Flipse, C.; Jansen, A.; van Santen, R.; Sautet, P., NO structures adsorbed on Rh (111): Theoretical approach to high-coverage STM images. *Physical Review B* **2006,** *73*, (24), 245408.
13. Zeng, Z.-H.; Da Silva, J. L. F.; Li, W.-X., Theory of nitride oxide adsorption on transition metal (111) surfaces: a first-principles investigation. *Physical Chemistry Chemical Physics* **2010,** *12*, (10), 2459-2470.
14. Nanba, T.; Kohno, C.; Masukawa, S.; Uchisawa, J.; Nakayama, N.; Obuchi, A., Improvements in the N2 selectivity of Pt catalysts in the NO–H2–O2 reaction at low temperatures. *Applied Catalysis B: Environmental* **2003,** *46*, (2), 353-364.
15. Wang, G.; Hove, M. A. V.; Ross, P. N.; Baskes, M. I., Monte Carlo simulations of segregation in Pt-Ni catalyst nanoparticles. *The Journal of Chemical Physics* **2005,** *122*, (2), 024706.
16. Mukerjee, S.; Srinivasan, S.; Soriaga, M. P.; McBreen, J., Role of Structural and Electronic Properties of Pt and Pt Alloys on Electrocatalysis of Oxygen Reduction: An In Situ XANES and EXAFS Investigation. *Journal of The Electrochemical Society* **1995,** *142*, (5), 1409-1422.
17. Hensley, A. J. R.; Schneider, S.; Wang, Y.; McEwen, J.-S., Adsorption of aromatics on the (111) surface of PtM and PtM3 (M = Fe, Ni) alloys. *RSC Advances* **2015,** *5*, (104), 85705-85719.
18. Yan, Z.; Wang, M.; Liu, J.; Liu, R.; Zhao, J., Glycerol-stabilized NaBH4 reduction at room-temperature for the synthesis of a carbon-supported PtxFe alloy with superior oxygen reduction activity for a microbial fuel cell. *Electrochimica Acta* **2014,** *141*, 331-339.
19. Lima, F. H. B.; Salgado, J. R. C.; Gonzalez, E. R.; Ticianelli, E. A., Electrocatalytic Properties of PtCo ／ C and PtNi ／ C alloys for the Oxygen Reduction Reaction in Alkaline Solution. *Journal of The Electrochemical Society* **2007,** *154*, (4), A369-A375.
20. Loukrakpam, R.; Luo, J.; He, T.; Chen, Y.; Xu, Z.; Njoki, P. N.; Wanjala, B. N.; Fang, B.; Mott, D.; Yin, J.; Klar, J.; Powell, B.; Zhong, C.-J., Nanoengineered PtCo and PtNi Catalysts for Oxygen Reduction Reaction: An Assessment of the Structural and Electrocatalytic Properties. *The Journal of Physical Chemistry C* **2011,** *115*, (5), 1682-1694.
21. Zou, L.; Fan, J.; Zhou, Y.; Wang, C.; Li, J.; Zou, Z.; Yang, H., Conversion of PtNi alloy from disordered to ordered for enhanced activity and durability in methanol-tolerant oxygen reduction reactions. *Nano Research* **2015,** *8*, (8), 2777-2788.
22. Strasser, P.; Koh, S.; Anniyev, T.; Greeley, J.; More, K.; Yu, C.; Liu, Z.; Kaya, S.; Nordlund, D.;

Ogasawara, H.; Toney, M. F.; Nilsson, A., Lattice-strain control of the activity in dealloyed core–shell fuel cell catalysts. *Nature Chemistry* **2010,** *2*, 454.

23. El-Deeb, H.; Bron, M., Microwave-assisted polyol synthesis of PtCu/carbon nanotube catalysts for electrocatalytic oxygen reduction. *Journal of Power Sources* **2015,** *275*, 893-900.
24. Wittkopf, J. A.; Zheng, J.; Yan, Y., High-Performance Dealloyed PtCu/CuNW Oxygen Reduction Reaction Catalyst for Proton Exchange Membrane Fuel Cells. *ACS Catalysis* **2014,** *4*, (9), 3145-3151.
25. Liao, Y.; Yu, G.; Zhang, Y.; Guo, T.; Chang, F.; Zhong, C.-J., Composition-Tunable PtCu Alloy Nanowires and Electrocatalytic Synergy for Methanol Oxidation Reaction. *The Journal of Physical Chemistry C* **2016,** *120*, (19), 10476-10484.
26. Cao, X.; Wang, N.; Jia, S.; Shao, Y., Detection of Glucose Based on Bimetallic PtCu Nanochains Modified Electrodes. *Analytical Chemistry* **2013,** *85*, (10), 5040-5046.